INL REPORT

INL/EXT-16-39120
Unlimited Release
Printed June 2016

Updates to the Generation of Physics Data Inputs for MAMMOTH Simulations of the Transient Reactor Test Facility - FY2016

Javier Ortensi, Benjamin Baker, Sebastian Schunert, Yaqi Wang, Frederick N. Gleicher, Mark D. DeHart

Prepared by
Idaho National Laboratory
Idaho Falls, Idaho 83415

The Idaho National Laboratory is a multiprogram laboratory operated by
Battelle Energy Alliance for the United States Department of Energy
under DOE Idaho Operations Office. Contract DE-AC07-05ID14517.

Issued by the Idaho National Laboratory, operated for the United States Department of Energy by Battelle Energy Alliance.

INL/EXT-16-39120
Unlimited Release
Printed June 2016

Updates to the Generation of Physics Data Inputs for MAMMOTH Simulations of the Transient Reactor Test Facility - FY2016

Javier Ortensi[1], Benjamin Baker[1], Sebastian Schunert[2],
Yaqi Wang[2], Fredrik N. Gleicher[1], Mark D. DeHart[1]

[1]Reactor Physics Design and Analysis
Idaho National Laboratory
P.O. Box 1625
Idaho Falls, ID 83415-3840

[2]Nuclear Engineering Methods and Development
Idaho National Laboratory
P.O. Box 1625
Idaho Falls, ID 83415-3840

Contents

Figures

Tables

1 Introduction

The Transient Reactor Test Facility (TREAT) is an air-cooled, thermal-spectrum test facility designed to evaluate reactor fuels and structural materials under simulated nuclear excursions and transient power/cooling mismatch situations in a nuclear reactor [1]. The U.S. Department of Energy Office of Nuclear Energy (DOE/NE) is preparing to resume operation of TREAT, which is located at Idaho National Laboratory (INL), by 2018 [2].

The INL is currently evolving the modeling and simulation (M&S) capability that will enable improved core operation as well as design and analysis of TREAT experiments. This M&S capability primarily uses MAMMOTH [3], a reactor physics application being developed under the award-winning [4] Multi-physics Object Oriented Simulation Environment (MOOSE) framework [5]. MAMMOTH allows the coupling of a number of other MOOSE-based applications.

The primary goal of TREAT transient simulation in the first year of the project was to demonstrate MAMMOTH power transient simulations with coupled transport/heat transfer calculations [6, 7]. The data and analysis capability needs identified during the first year of research include:

- the generation of a deterministic reference solution for the full core,
- the preparation of anisotropic diffusion coefficients,
- the testing of the SPH equivalence method,
- and the improvement of the control rod modeling.

These items are all addressed in this second year of work. In addition, a detailed analysis of historical data was conducted earlier this year [8], which proposed a focus on the validation work for MAMMOTH consisting of comparing data from the M8 [9] and AN [10] calibrations. In addition to the aforementioned research items, this report includes the progress made in the modeling of the M8 core configuration and experiment vehicle since January of this year.

The MAMMOTH team at the Idaho National Laboratory is proposing a novel analysis approach that consists of using full core Monte Carlo steady state calculations to prepare cross section tabulations, which are subsequently used in deterministic transient simulations of TREAT using diffusion theory.

2 Computer Codes

Serpent 2 [11] is a three-dimensional continuous-energy Monte Carlo reactor physics code developed at VTT Technical Research Centre of Finland. It was selected as the main cross section preparation tool for this project because it offers 3-D spatial homogenization and group constant generation for deterministic reactor simulator calculations. At the same time, Serpent 2 provides a detailed reference calculation without energy, angular, or spatial discretization error. Serpent has been in use at the Idaho National Laboratory since 2010 [12, 13]. The neutron cross sections used in Serpent 2 are based on ENDF/B-VII.1.

The reactor physics application MAMMOTH has been designed and implemented using the MOOSE environment [5]. MAMMOTH allows the coupling of a number of other MOOSE-based applications including: Rattlesnake [14] for neutron transport, RELAP-7 [15] for low-resolution thermal-fluids, and BISON [16] for fuel performance analyses. In general MAMMOTH has great flexibility to solve complex reactor multi-physics problems. One approach is by solving a large system of interlinked nonlinear equations on the same mesh. These equations can be simultaneously solved with the Jacobian-Free Newton-Krylov (JFNK) method [17, 18]. The MOOSE framework provides the necessary flexibility to perform multi-scale modeling where necessary, which will be imperative in experiment analysis and design. The general long-term technical objective of the currently funded MAMMOTH project in support of TREAT is to develop a set of high-resolution reactor physics and fuels performance models that can accurately predict the transient behavior of an in-core experiment as driven by a reactor transient.

The Rattlesnake [14] neutron transport solver incorporates a variety of spatial and angular discretizations including diffusion, P_N and S_N. In this report the primary solvers used are the Self Adjoint Angular Flux (SAAF) formulation of the S_N equation and diffusion. It is important to note that the SAAF-S_N in Rattlesnake includes a void treatment [19] that enables its application in TREAT simulations.

The generation of the various meshes is accomplished with specialized Python scripts that access the API interface in Cubit [20].

3 New Methodologies

A departure from the traditional analysis approach, which normally consists of lattice followed by full core calculations, is currently being pursued at INL. Full core Serpent Monte Carlo steady state calculations are instead employed to prepare the cross section tabulations, thus guaranteeing that the cross sections in the various regions of the core are appropriately weighted. These tabulations are subsequently used in deterministic transient simulations of TREAT using the diffusion solver in Rattlesnake.

Previous research indicated two deficiencies that adversely affect the power distribution in the TREAT active core region: 1) the axial streaming in the air channels that surround each element and 2) the lack of an equivalence procedure to preserved reaction rates in controlled elements. Furthermore, the M8 calibration configuration also includes a half slotted core with large void channels and an experiment vehicle with significant void regions. Currently Serpent does not have the capability to generate anisotropic diffusion coefficients to allow better modeling of neutron streaming effects with a diffusion solver. To address this issue a methodology was implemented in the Rattlesnake transport solver, which is the topic discussed in Subsection 3.1. The second topic, Subsection 3.2, addresses the need for an equivalence procedure to ensure preservation of the reaction rates between the reference Monte Carlo model and the cross section set used in the MAMMOTH models. The final data preparation sequence proposed entails the generation of various cross section tabulations with Serpent, followed by the calculation of anisotropic diffusion coefficients and, finally, the equivalence correction of the cross sections with SPH, as delineated in Figure 1. Rattlesnake automatically generates a new tabulation after each step without the need to use multiple datasets or other cumbersome data processing.

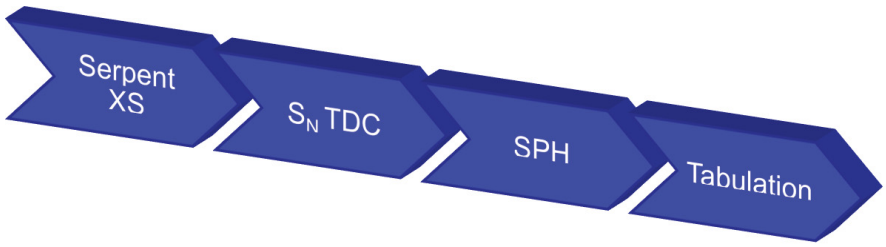

Figure 1: Cross section preparation sequence for TREAT

3.1 Directional Diffusion Coefficients

The computation of region-wise directional (anisotropic) diffusion coefficients can be readily implemented for optically think media with optically thin channels [21, 22]. In this formulation, one can calculate a diffusion tensor using a deterministic transport solution.

The region-wise diffusion tensor is defined as

$$[\bar{\bar{D}}]_{i,j} = \frac{1}{4\pi}\int_{4\pi} d\Omega_i \Omega_j f \tag{1}$$

where the function f is obtained from a source problem with the transport streaming and collision operators and a unit source

$$\vec{\Omega}\cdot\nabla f_g + \Sigma_{t,g} f_g(r,\vec{\Omega}) = 1. \tag{2}$$

Unfortunately, this method does not allow for the spatial homogenization of regions, which would enable the computation of effective tensor diffusion coefficients for the full radial homogenization of the element model. Instead, the current approach relies on SPH to help correct the streaming in the air channels for these models. Nevertheless, the tensor diffusion coefficients are needed in the experiment vehicle and the slotted assemblies.

3.2 Superhomogenization

The superhomogenization (SPH) method is a cross section correction scheme that reduces errors from spatial homogenization and was first introduced by Kavenoky [23] and generalized by Hébert [24]. This technique uses SPH factors as the only homogenization parameter to correct the cross sections, which fits very well with the continuous finite element method (FEM) used in various Rattlesnake solvers. In diffusion theory, the SPH corrected cross sections are defined for each macro region m and energy group g as:

$$\tilde{\Sigma}_{m,g} = \mu_{m,g}\Sigma^{ref}_{m,g} \tag{3}$$

where the tilde ($\sim$) superscript represents values from the macro calculation and "ref" superscript represents reference values. The SPH factors are defined to preserve the reaction rate between the macro and reference calculations. They also need to be normalized for eigenvalue problems to obtain a unique set of solutions, usually volume weighed average fluxes for each energy group. The SPH factor and normalized SPH factor are defined by:

$$\mu_{m,g} = \frac{\phi^{ref}_{m,g}}{\tilde{\phi}_{m,g}} \qquad\qquad \mu_{m,g} = \frac{\phi^{ref}_{m,g}}{\tilde{\phi}_{m,g}}\frac{\bar{\bar{\phi}}_g}{\bar{\phi}^{ref}_g} \tag{4}$$

A source problem is solved to compute the SPH factors, which takes the following form for the

multi-group diffusion equation:

$$-\nabla \cdot \mu_{m,g} D_{m,g} \nabla \phi_{m,g} + \mu_{m,g} \Sigma^{r}_{m,g} \phi_{m,g} = \frac{\chi_g}{k_{eff}} \sum_{g'=1}^{G} \mu_{m,g'} \nu \Sigma_{f_{m,g'}} \phi_{m,g'} + \sum_{g' \neq g}^{G} \mu_{m,g'} \Sigma^{g \leftarrow g'}_{s0_m} \phi_{m,g'} \qquad (5)$$

The resulting system of coupled equations is non-linear, since the SPH factors depend on the flux calculation and, in turn, the fluxes depend on the SPH factors through the cross sections. The initial guess is set by using the macro region fluxes and k_{eff} from the reference calculation. The traditional way of solving this problem [25, 26, 27, 28, 29, 30, 31] employs a Picard (fixed-point) iterative process, which will be referred to as "SPH iteration." This approach was implemented within the MAMMOTH application with a dedicated solver containing an outer SPH iteration that calls the linear system system solver, normalizes the fluxes and computes the updated SPH factors until the SPH factor convergence criteria is met.

The novel approach, referred here as "PJFNK SPH," involves the use of MOOSE's non-linear solver with the Preconditioned Jacobian-free Newton-Krylov method (PJFNK) [32, 18, 17], which is a combination of Newton and a Krylov subspace iterative method. The normalization of fluxes and computation of the updated SPH factors occurs at every linear residual evaluation, thereby accelerating the convergence of the algorithm. With this approach, it is important that the initial guess is within the Newton convergence radius. In order to improve the initial guess, the MOOSE MultiApp system is used to spawn an initial "free SPH iteration" calculation with a limited number of iterations. The solution from this initial guess calculation is then transferred, via the MOOSE Transfer system, to set the initial guess for the PJFNK method. The SPH factors obtained from both methods were verified to be identical, within the convergence criteria.

Furthermore, it is well established that equivalence theory applied to homogenized reflectors is difficult and the convergence of the problem worsens with more than two groups [33, 24, 34]. In addition, the presence of void boundary conditions can exacerbate the already poor convergence. The PJFNK SPH solver is very robust and can circumvent these pitfalls with the appropriate use of the free SPH iterations.

4 Models and Meshing

This section discusses a set of problems developed to test the methodologies implemented in Rattlesnake based on the modeling needs identified in previous research. The problems test the control rod and the slotted element. These smaller problems serve as a preliminary step to better understand the methodologies that will be applied to the full modeling of the current TREAT core configuration. The model for the M8 calibration core is discussed in the last subsection. The improvements include modifications to the cross section models and the meshing scripts for these configurations.

4.1 Control Rod Element Supercell

This first problem consists of a 3 by 3 supercell problem, shown in Figures 2 and 3, with a control rod element positioned in the center and surrounded by standard fuel elements. The cross sections obtained from the Serpent model are fully homogenized in the radial direction in each element with 13 axial locations identified in previous research to capture the reflector effects [6]. Furthermore, the cross sections for the face and diagonally adjacent standard elements are segregated in order to better model the geometry. This supercell includes axial graphite reflectors on top and bottom of the active core, where a vacuum boundary is imposed. Two configurations with control rod fully inserted and withdrawn are studied. The fully inserted and full length of travel of the control rod is consistent with the shutdown and safety rods.

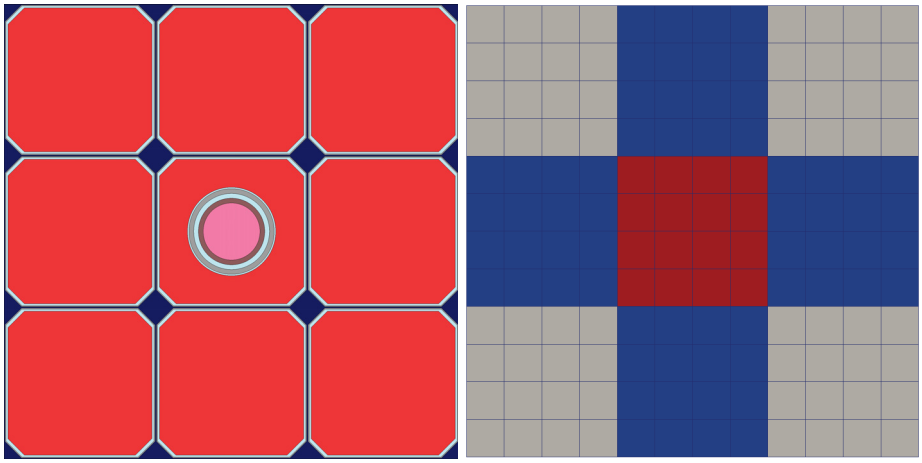

(a) Serpent **(b)** MAMMOTH Mesh

Figure 2: X-Y plane geometry and mesh for the 3x3 supercell. B_4C poison region shown in pink. (Not to scale)

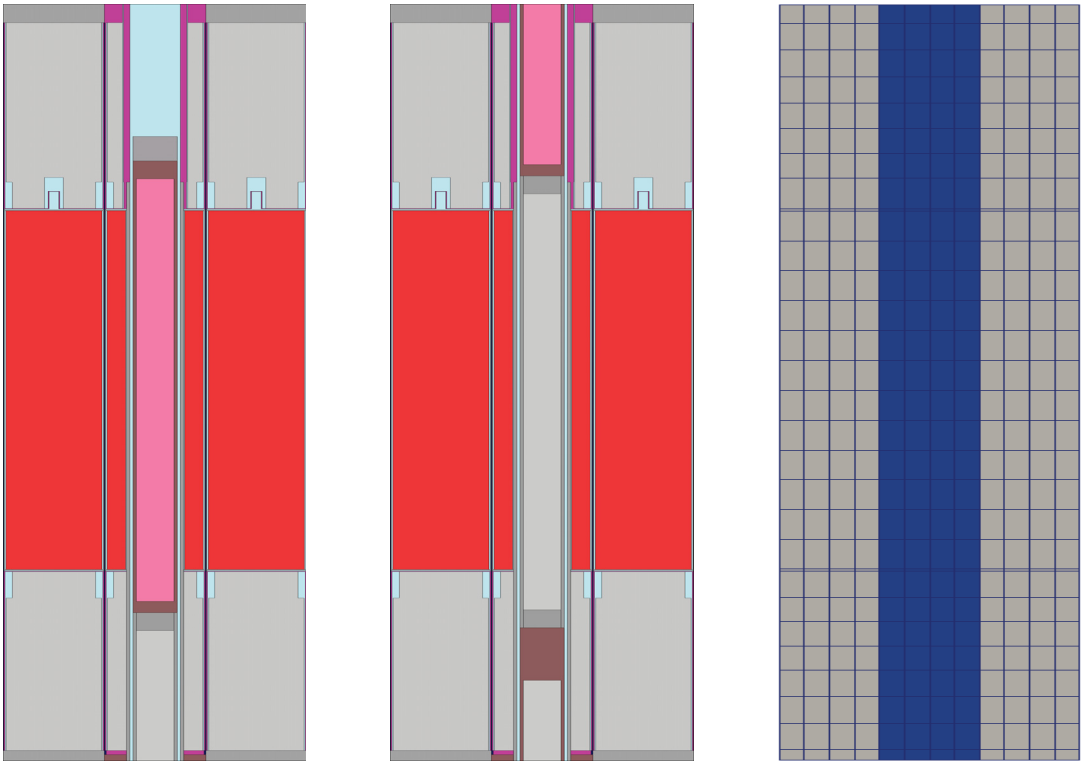

(a) Serpent - Inserted **(b)** Serpent - Withdrawn **(c)** MAMMOTH Mesh

Figure 3: X-Z plane geometry and mesh for the 3x3 supercell

These control rods used in TREAT constitute strong absorber regions where diffusion theory breakdowns. Furthermore, the radial homogenization of the control rod region with the rest of the element, which includes fuel, introduces homogenization errors that can be very large in magnitude. The SPH method can be used in these control rod elements to preserve the transport reaction rates. As a contingency measure, the capability to homogenized the cross sections in the control region and the corresponding mesh have also been developed as shown in Figure 4.

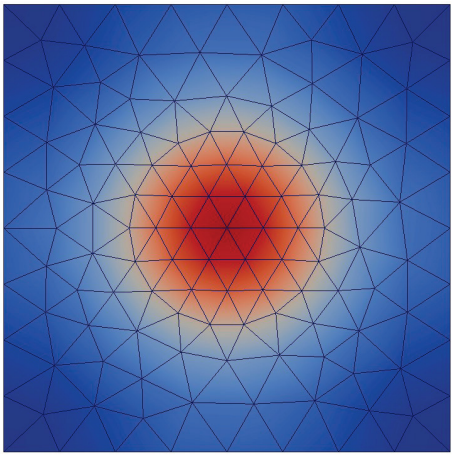

Figure 4: Explicit modeling of the control rod region - Thermal Flux

4.2 Slotted Element Supercell

The next test problem consists of a 5 by 5 supercell with slotted assemblies, which is a similar configuration as the one in the M8 calibration and the current core, but without the experiment vehicle. The slotted assemblies constitute an additional layer complexity for diffusion theory, since it requires the calculation of directional diffusion coefficients in order to model the streaming of neutrons in void regions. The methodology introduced in Section 3.1 is tested in this configuration. The Serpent geometric model and the MAMMOTH mesh are shown in Figures 5 and 6. Just as in the previous test the elements are radially homogenized with 13 axial cross section regions. Separate cross sections are prepared for one standard fuel element and one slotted element.

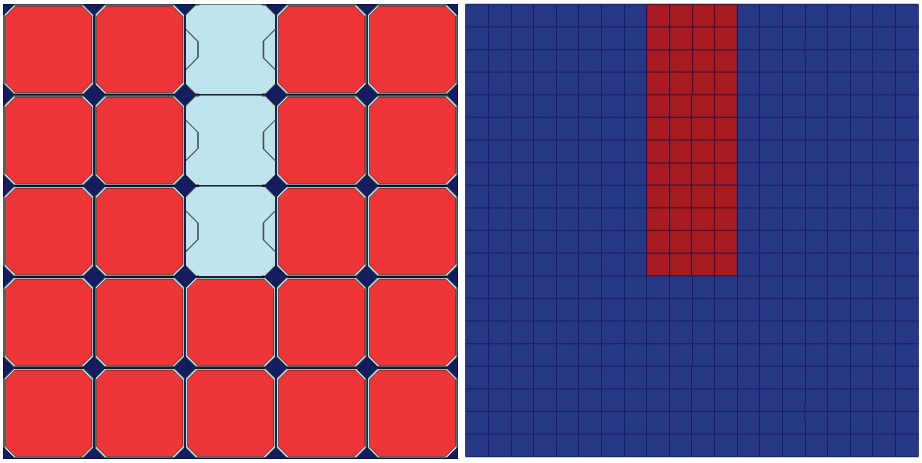

(a) Serpent **(b)** MAMMOTH Mesh

Figure 5: X-Y plane geometry and mesh for the 5x5 supercell. (Not to scale)

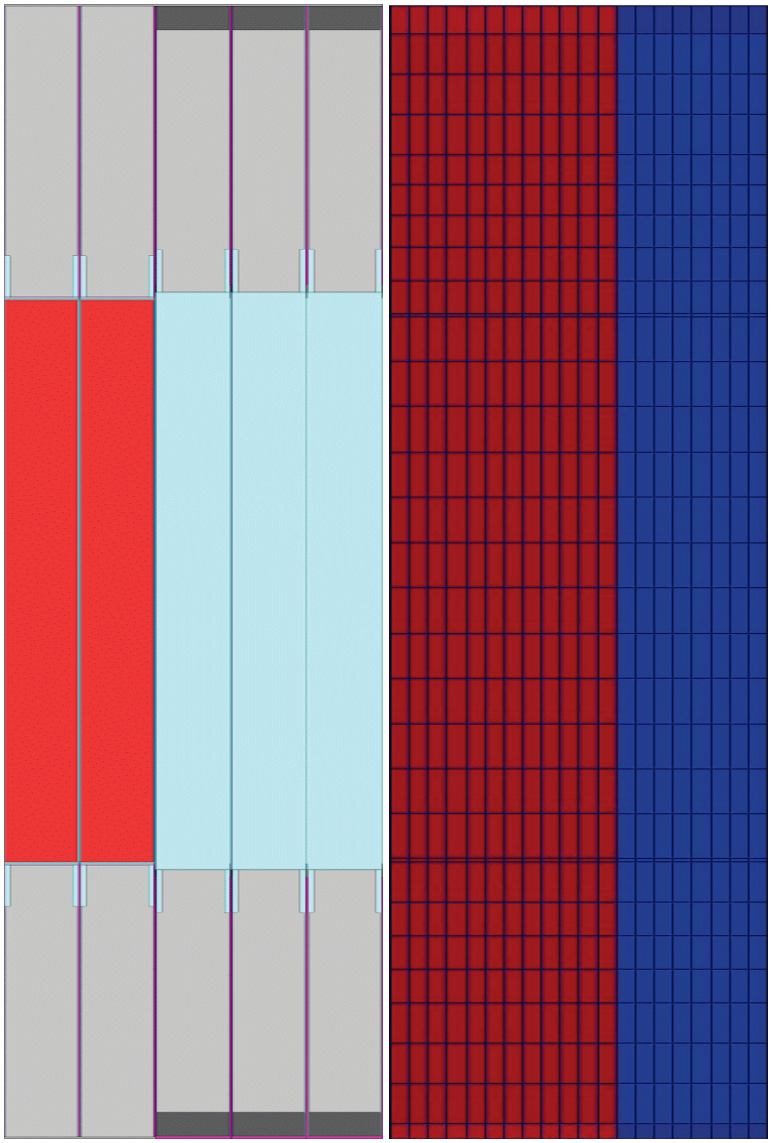

(a) Serpent **(b)** MAMMOTH Mesh

Figure 6: Y-Z plane geometry and mesh for the 5x5 supercell. (Not to scale)

4.3 M8 Calibration Core

The M8 calibration half slotted core was modeled in Serpent to prepare cross sections. Initially, the core was modeled without the experiment hardware due to its complexity. It was found that the eigenvalue was in disagreement with the critical experiment by roughly 4700 pcm. It was later discovered that the experiment zone, which includes a Dysprosium filter surrounding the experiment, was the major source of the error. Cross sections were prepared by homogenizing radially a number of independent regions. These include control rod elements, slotted and half slotted elements, various standard assemblies (based on radial positions), and the M8 experiment vehicle. A comparison of the Serpent geometric model and the MAMMOTH mesh is included in

Figures 7 and 8. Some of these cross section regions can be observed in the MAMMOTH mesh with distinct coloring.

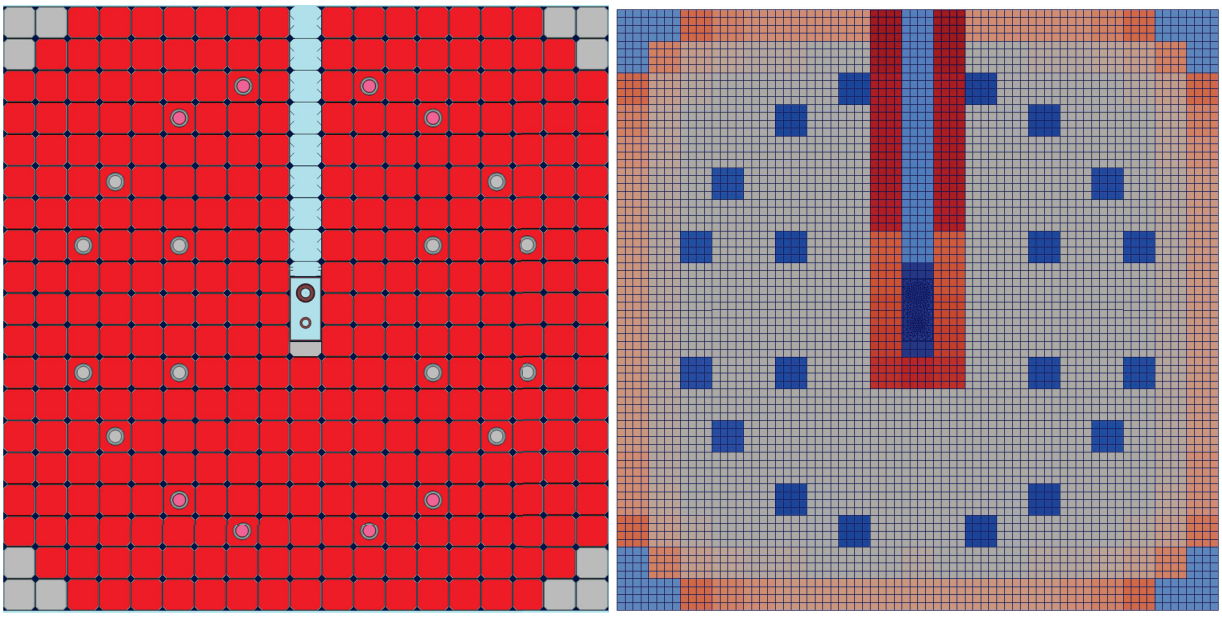

(a) Serpent **(b)** MAMMOTH Mesh

Figure 7: X-Y plane geometry and mesh for the M8 TREAT 19x19 core region. (Not to scale)

Additional detail on the modeling of the experiment vehicle is provided in Figure 9. The Serpent model includes the explicit Dysprosium filter surrounding the experiment. One of the major challenges for cross-section development using Monte Carlo methods occurs in regions with small volumes. This is the case for the cross-section development of the flux wire. The flux wire was 0.102 cm (0.040 inches) in diameter and 152.4cm (60 inches) long compared to the entire domain. In traditional Monte Carlo, the method of obtaining better statistics for these small regions is to either increase the number of particles or use variance reduction techniques. Variance reduction techniques are not available in Serpent at this point and the number of particles/cycles had to be increased. To improve the statistics, an equivalent fuel pin with equal mass was smeared throughout the entire wire holding assembly to increase the volume, which in turn produced better statistics.

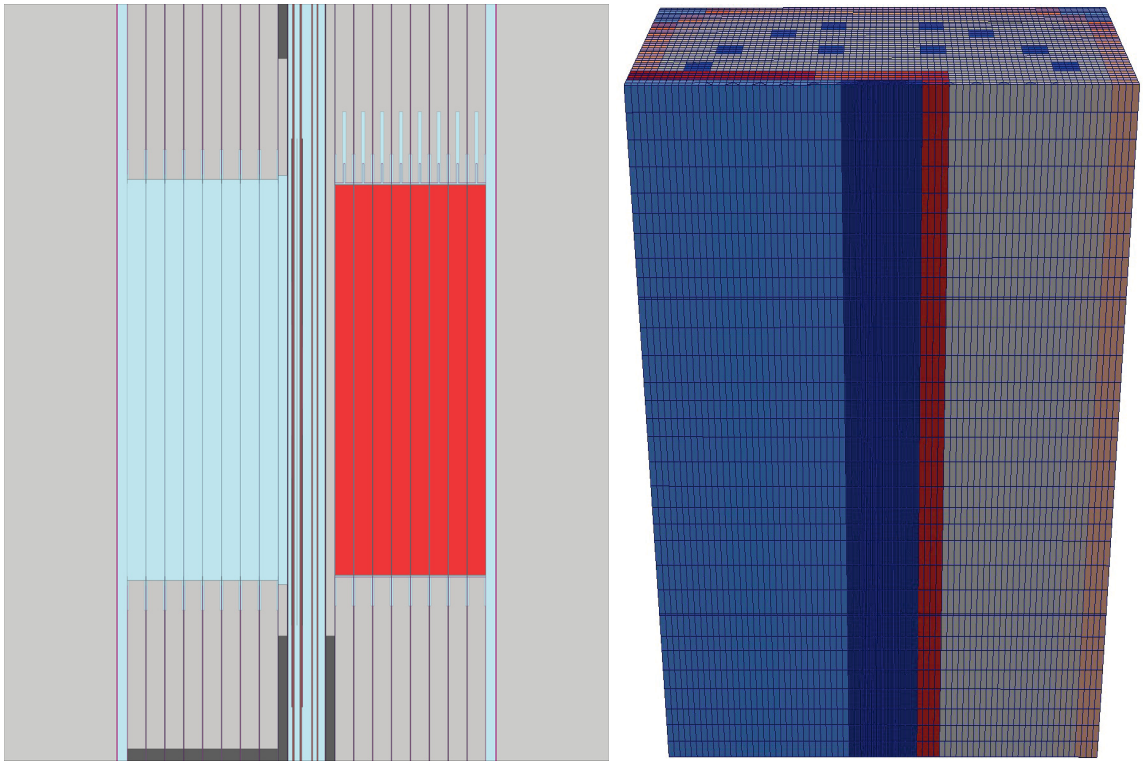

(a) Serpent **(b)** MAMMOTH Mesh

Figure 8: Y-Z plane geometry and mesh for the M8 TREAT 19x19 core region. (Not to scale)

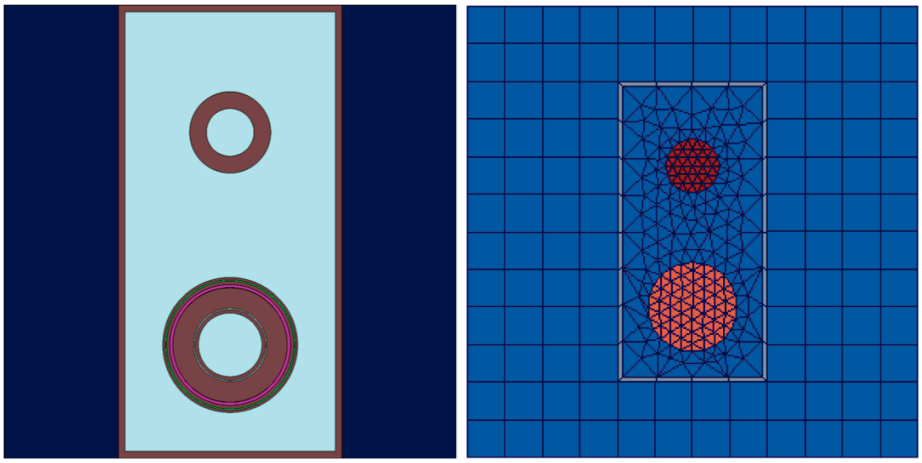

(a) Serpent **(b)** MAMMOTH Mesh

Figure 9: X-Y plane geometry and mesh for the M8 vehicle. (Not to scale)

5 Results

5.1 Control Rod Element Supercell

The eigenvalue and balance table for the reference Serpent calculations is included in Table 1. The numerical comparison of the two SPH schemes are shown in Table 2. The results indicate that a minimum of 1 and 4 initial free SPH iterations are required to converge the PJFNK SPH solutions for the 4 and 11 group problems, respectively. The PJFNK SPH approach is significantly faster than the traditional SPH iteration (a factor of 10 for the 4 group problem and a factor of 45 for the 11 group problem). To optimize the PJFNK SPH convergence, one must determine the number of free SPH iterations that ensure convergence and minimize the computational time. Table 2 shows that the optimal number of free SPH iterations was slightly higher than the minimum number of free SPH iterations. The convergence behavior of the PJFNK SPH solver for this problem is included in Figure 10.

Table 1: Reference reaction rates for the 3x3 supercell

Control Rod	k_{eff} ($\pm$pcm)	Fission Source Rate	Absorption Rate	Leakage Rate
Withdrawn	1.34888 ($\pm$1.00)	1.1168E+14	1.0976E+14	1.9191E+12
Inserted	0.67320 ($\pm$2.20)	2.2379E+14	2.1852E+14	5.2638E+12

Table 2: SPH calculations with control rod inserted

Solver	Number of Energy Groups	Free SPH Iterations	CPU time [sec]
SPH iteration	4	-	660.0
PJFNK SPH	4	3	60.7
SPH iteration	11	-	9280.0
PJFNK SPH	11	5	202.9

The eigenvalue and balance table for the MAMMOTH solutions in 4 and 11 energy groups are included in Tables 3 and 4. The case with the control rod withdrawn shows improvement with SPH corrected cross sections. The error in the fission and absorption source rates dropped by a factor of 2.9 and 35, respectively, in the 4 group calculation. The error in the fission and absorption source rates dropped by a factor of 3.5 and 82, respectively, in the 11 group calculation. Note that the eigenvalues are not strictly preserved because of the vacuum boundary condition and the use of the diffusion operator, which becomes apparent in the leakage rate error. Nevertheless, the leakage is two orders of magnitude lower than absorption and fission, thus the larger error is unimportant.

These improvements are even more dramatic with the control rod fully inserted, where a misprediction of nearly -6,300 pcm is reduced to 378 pcm. The error in the fission source and absorption

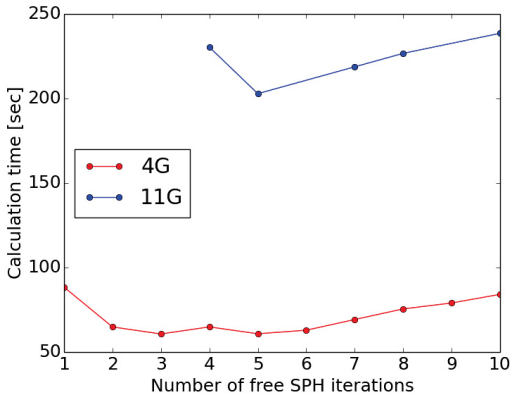

Figure 10: Convergence of the PJFNK SPH with free SPH iterations

Table 3: Diffusion results with 4 coarse energy groups for the 3x3 supercell

Control Rod	SPH	k_{eff} (pcm)	Fission Source Rate [% Difference]	Absorption Rate [% Difference]	Leakage Rate [% Difference]
Withdrawn	No	1.36036 (850.7)	-0.851	-0.418	-25.438
Withdrawn	Yes	1.35276 (287.7)	-0.295	-0.012	-16.307
Inserted	No	0.63081 (-6296.85)	6.029	6.663	-20.174
Inserted	Yes	0.67574 (378.39)	-0.415	-0.093	-13.653

Table 4: Diffusion results with 11 coarse energy groups for the 3x3 supercell

Control Rod	SPH	k_{eff} (pcm)	Fission Source Rate [% Difference]	Absorption Rate [% Difference]	Leakage Rate [% Difference]
Withdrawn	No	1.36275 (1028.4)	-1.025	-0.494	-31.273
Withdrawn	Yes	1.35278 (289.3)	-0.296	0.006	-17.383
Inserted	No	0.63081 (-6296.85)	7.406	6.708	-22.149
Inserted	Yes	0.67574 (378.39)	-0.062	-0.389	-13.851

rate drops a factor of 14.5 and the 71.65, respectively, in the 4 group calculation.The error in the fission source and absorption rate drops a factor of 119.5 and the 17.2, respectively, in the 11 group calculation. The axially averaged radial power distribution (RPD) with nominal cross sections is shown in Figure 11. The RPD with SPH corrected cross sections is shown in Figure 12. The 11 group solution shows the best agreement with the reference results, but even the maximum error for the full distribution in the 4 group results is within 1.15% of the Monte Carlo reference.

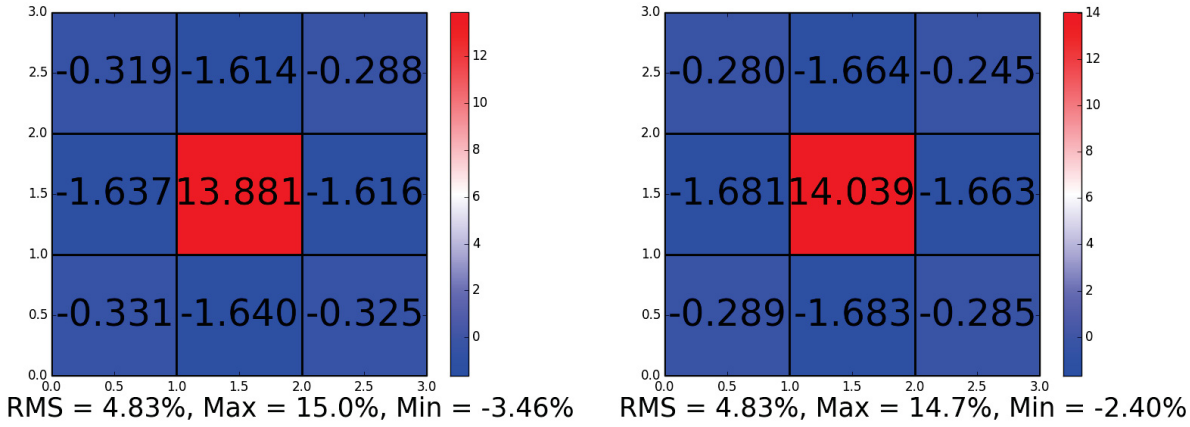

(a) 4 Group **(b)** 11 Group

Figure 11: % Difference in the RPD with the control rod inserted

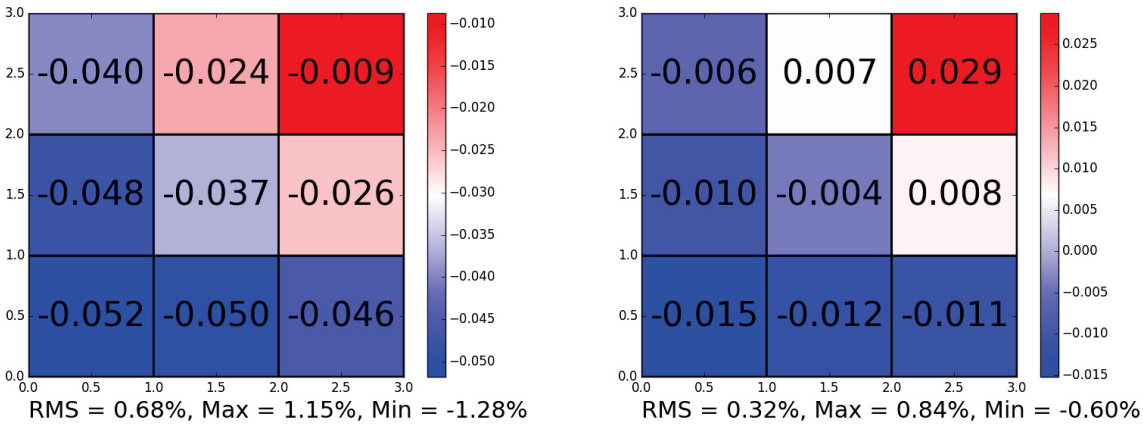

(a) 4 Group **(b)** 11 Group

Figure 12: % Difference in the RPD with the control rod inserted (SPH corrected)

5.2 Slotted Element Supercell

The eigenvalue and balance table for the reference Serpent calculation is included in Table 5. Examples of the computed tensor diffusion coefficients for the fast and thermal groups using the SAAF-S_N solver in Rattlesnake are shown in Figures 13 and 14. The results indicate small effects in the x component for both energy groups but large components in the y and z directions, which are consistent with the location of the slotted assemblies in the geometry.

Table 5: Reference reaction rates for the 5x5 supercell

k_{eff} (±pcm)	Fission Source Rate	Absorption Rate	Leakage Rate
1.35115 (±5.00)	5.5743E+12	5.3207E+12	2.5354E+11

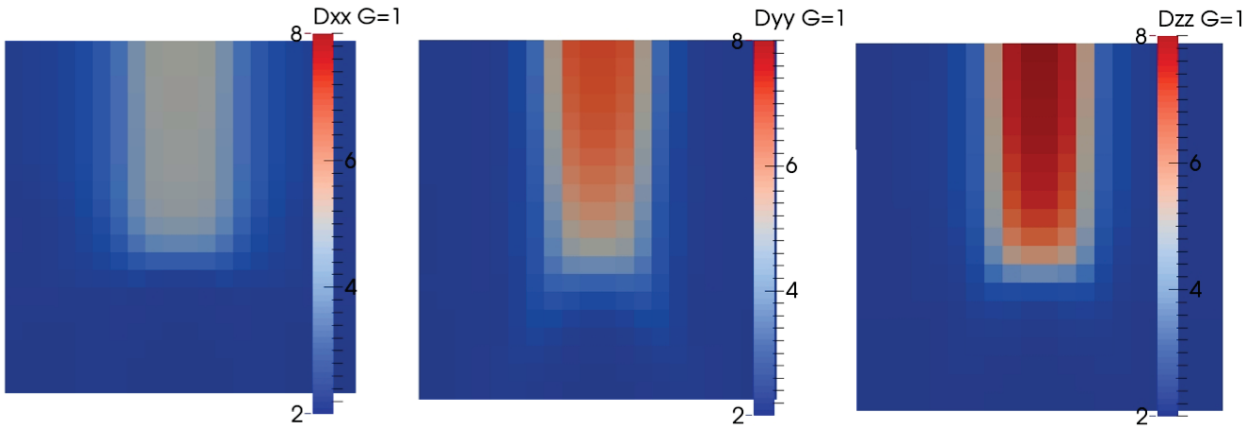

Figure 13: Tensor Diffusion Coefficients in the fast group (midplane)

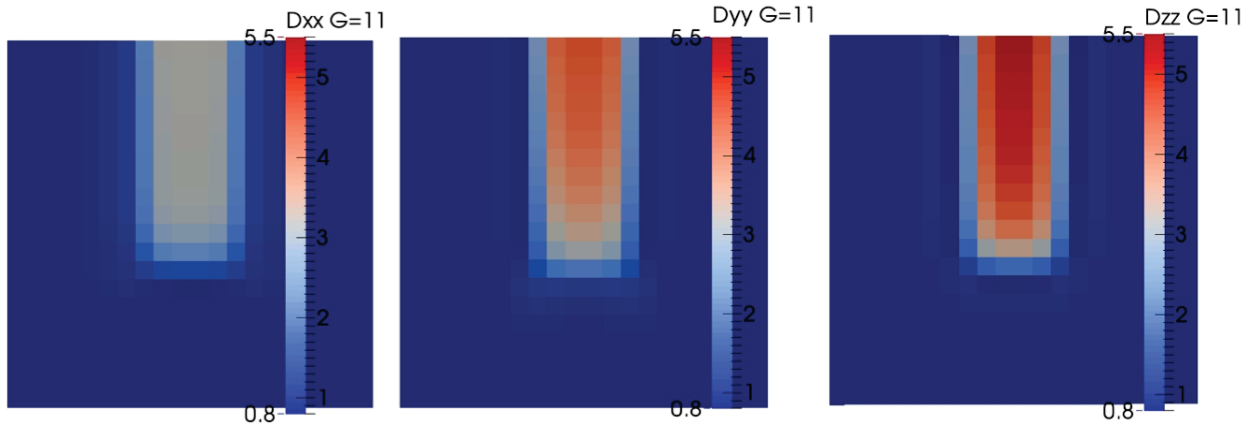

Figure 14: Tensor Diffusion Coefficients in the thermal group (midplane)

The numerical comparison to several MAMMOTH simulations with diffusion are included in Table 6. The solution using the cross section library containing the original transport cross sections

from Serpent is labeled ”nominal.” The results obtained using the SPH corrected cross sections are labeled ”SPH” and the cross sections that include both a tensor diffusion coefficient and the SPH are labelled ”TDC-SPH.” The nominal case considerably overpredicts the fission source and absorption rates. The leakage rate appears to be better than in the previous 3x3 case but this could be due to cancellation of error and boundary condition effects. The results obtained with the SPH and TDC-SPH corrections are very similar and significantly better than the original case.

Table 6: Difference in the MAMMOTH diffusion reaction rates for the 5x5 supercell vs. Serpent

Case	k_{eff} (±pcm)	Fission Source Rate	Absorption Rate	Leakage Rate
nominal	1.33685 (±-1058.0)	1.26%	1.07%	-3.07%
SPH	1.35625 (±377.6)	0.023%	-0.38%	-8.81%
TDC-SPH	1.35680 (±418.4)	0.024%	-0.42%	-9.72%

The effects of the corrections on the power distribution are included in Table 7. The ability to correct for streaming effects and the reaction rates leads to a significant improvement in the predicted power distribution with an RMS error below 1% and maximum and minimum errors within 2.5%. The planes with the peak errors for the nominal and TDC-SPH cases are shown in Figure 15. The error distribution is evenly distributed in the planes.

Table 7: Total power distribution metrics for the MAMMOTH diffusion solutions vs. Serpent

Case	RMS Difference	Maximum Difference	Minimum Difference
nominal	5.02%	9.56%	-6.34%
SPH	1.75%	2.96%	-3.73%
TDC-SPH	0.93%	1.82%	-2.42%

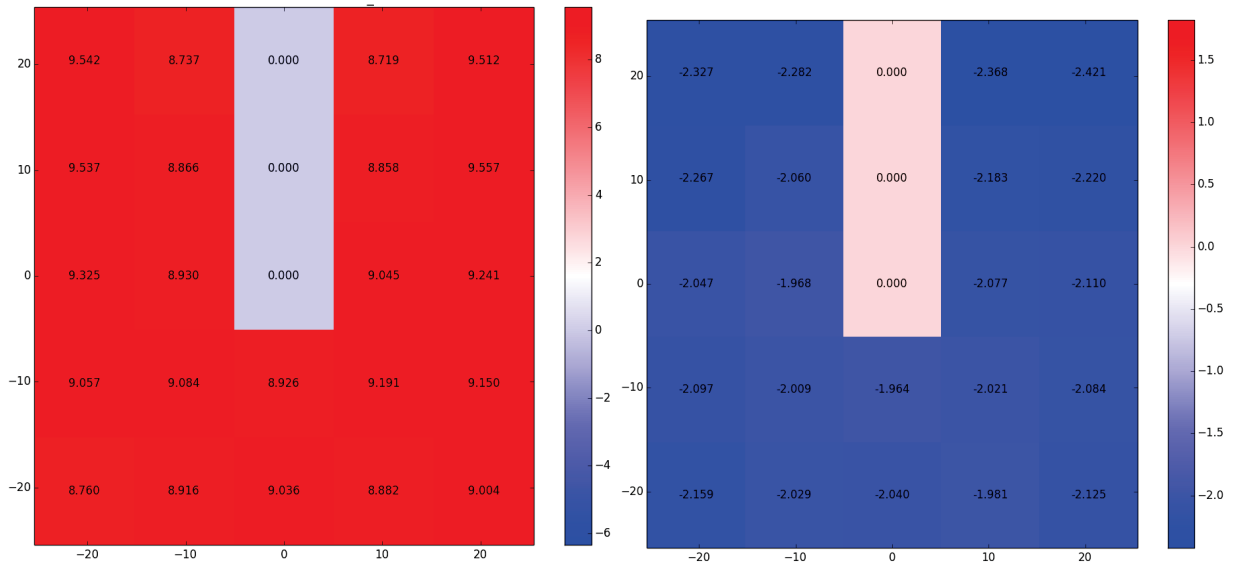

(a) nominal **(b)** TDC-SPH

Figure 15: % Difference in power distribution (plane with peak error)

5.3 M8 Calibration Core

The M8 calibration core is quite challenging to both Monte Carlo and deterministic codes for different reasons. The Monte Carlo code struggles with the generation of cross sections in small volume regions (flux wires) due to poor statistics, whereas for deterministic diffusion this core configuration combines all aspects that render diffusion theory outside of its range of applicability. Some of the key neutronic issues with the M8 configuration include:

- the presence of small volumes,
- the presence of a large number of control rods,
- half slotted core configuration (which also creates an asymmetric distribution) and
- a vehicle with a very strong absorber and significant void regions.

Since January 2016, the main effort has been focused on the M8 vehicle with flux wire measurements. The Serpent calculation was compared to the startup number 6544 on 24 August 1992 [9], which irradiated flux wire L91-60-1 at 80kW for 2 hours. Gamma rays were recorded from the flux wire to infer the axial power profile. The results of the relative gamma activity are shown below in Figure 16. The M8 Calibration data is shown with black triangles, since the figure also contains the results from the prior M2 calibration core (white squares). The Monte Carlo Serpent results were compared to the M8 calibration axial power profile to determine how well the Serpent model compared with the experimental values. These comparisons will also help establish the inherent bias in the Serpent model which should be incorporated to the MAMMOTH model. As shown

in the figure the shape obtained from the Serpent model agrees very well with the experimental measurements. Unfortunately, no magnitude values are available to perform comparisons.

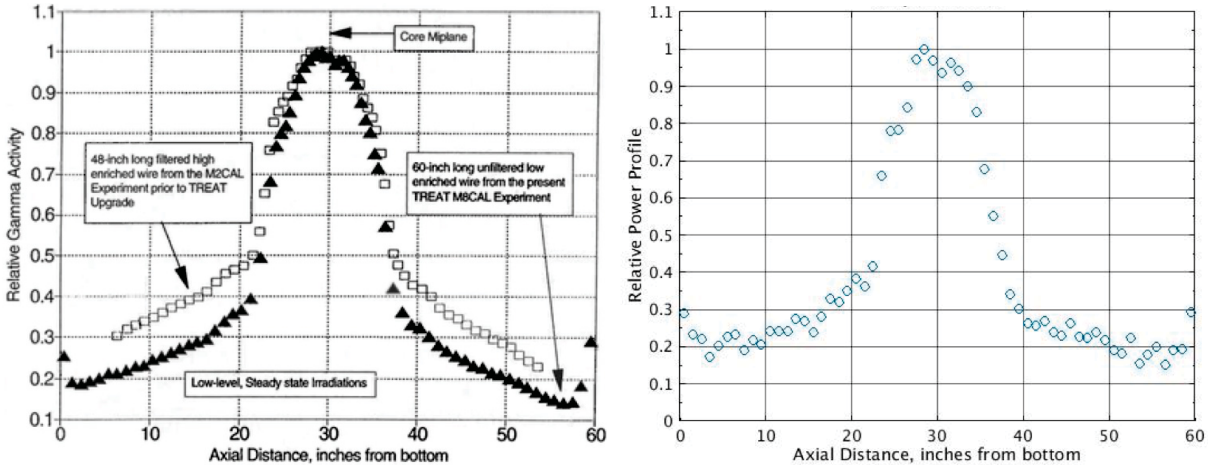

(a) Experimental **(b)** Serpent

Figure 16: Axial power profile comparisons with full-length flux monitor wires

The axial power profiles obtained with MAMMOTH using 1) the raw cross-sections from Serpent and 2) the same cross sections with TDCs, are compared to the Serpent detector tally results, Figure 17. The axial shape is dramatically improved when the TDCs are introduced a match very well the reference Serpent and experimentally measured axial distributions.

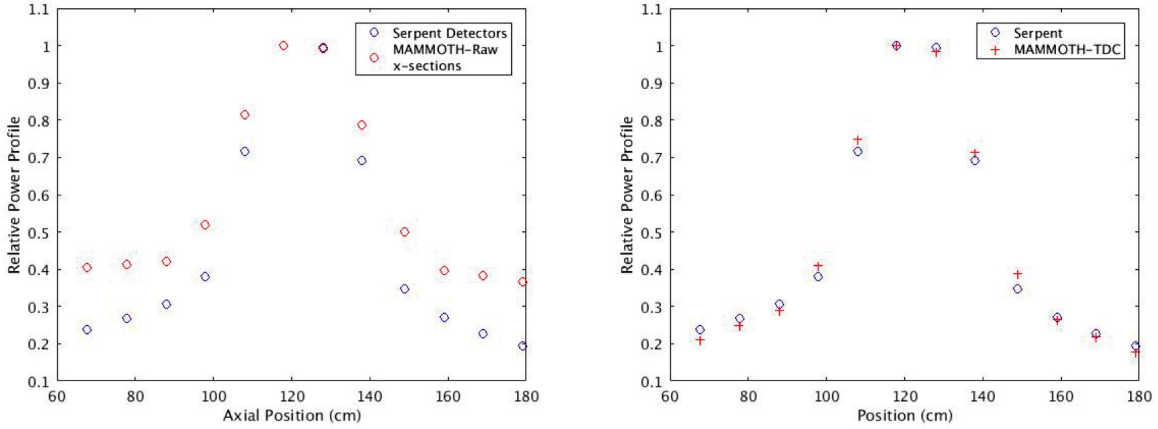

(a) Diffusion **(b)** TDC

Figure 17: Axial power profile simulation comparisons

The work on the M8 calibration core with the post-transient configuration is ongoing and requires significant improvements. The preliminary eigenvalues for this configuration are included in Table 8. The nominal diffusion solution (with the raw cross sections from Serpent) yields bad results, whereas the SPH corrected diffusion and S_N solutions produce eigenvalue differences that, albeit

similar, are large in magnitide (800 pcm). Further analysis of the power distribution in Table 9 indicates that the SPH corrected diffusion and SAAF-S_N solution produce similar results. This suggests that there are modeling issues that need to be addressed.

Table 8: M8 calibration post-transient configuration eigenvalues

Code	k_{eff}	pcm
Serpent	1.01867	$\pm$1.2
nominal	0.85873	-15701.3
SPH	1.02754	870.7
SAAF-S_N	1.02704	821.7

Table 9: M8 calibration post-transient configuration power distribution metrics

Code	RMS Difference in Power	Maximum Difference in Power	Minimum Difference in Power
nominal	26.90%	95.78%	-54.28%
SPH	7.93%	57.32%	-26.49%
SAAF-S_N	7.70%	57.96%	-23.62%

6 Conclusion

This work delineates the current data calculation sequence for TREAT, which entails a full core Serpent Monte Carlo cross section preparation step, followed by further improvement of the data with the calculation of tensor diffusion coefficients and, finally, the SPH corrected cross sections in Rattlesnake. These latter improvements where implemented and tested during FY2016. Neutron streaming regions in TREAT can now be solved with the diffusion solver. The results indicate that the treatment of the streaming in the slotted elements is necessary to produce axial distributions in the M8 experiment region that match those obtained from Monte Carlo simulations. The Superhomogenization procedure implemented in Rattlesnake allows for the preservation of reaction rates from the reference calculations, which enables improved modeling of the control rods, even with full homogenization of the region. The fission and absorption rates are improved by 15% for a fully homogenized control element in 4 and 11 groups. This also implies that further energy condensation is an option and can be pursued in the future. Furthermore, the new SPH PJFNK approach allows to converge problems that were intractable, or very difficult to converge, in the past. Finally, the work on the M8 calibration continues and improved results are expected by the end of the fiscal year.

References

[1] *TREAT, a Pulsed Graphite-Moderated Reactor for Kinetics Experiment*, volume 10, Geneva, Switzerland, 1958.

[2] U.S. Department of Energy. Mission Need Statement for the Resumption of Transient Fuel Testing, 2010.

[3] F.N. Gleicher and J. Ortensi et al. The Coupling of the Neutron Transport Application Rattlesnake to the Fuels Performance Application BISON. In *International Conference on Reactor Physics (PHYSOR 2014)*, Kyoto, Japan, May 2014.

[4] R&D Magazine. 2014 R&D 100 Award Winners, 2014.

[5] D. Gaston, C. Newman, G. Hansen, and D. Lebrun-Grand'e. Moose: A parallel computational framework for coupled systems of non-linear equations. *Nucl. Eng. Design*, 239(1768-1778), 2009.

[6] J. Ortensi, A. Alberti, Y. Wang, M.D. DeHart, F.N. Gleicher, S. Schunert, and T.S. Palrmer. Methodologies and Requirements for the Generation of Physics Data Inputs to MAMMOTH Transient Simulations in Support of the Transient Reactor Test Facility. Technical Report NL/LTD-15-36265, Idaho National Laboratory, September 2015.

[7] J. Ortensi, M.D. DeHart, F.N. Gleicher, Y. Wang, and S. Schunert. Full Core TREAT Kinetics Demonstration Using Rattlesnake/BISON Coupling within MAMMOTH. Technical Report INL/EXT-15-36268, Idaho National Laboratory, August 2015.

[8] B. Baker, J. Ortensi, M.D. DeHart, Y. Wang, F.N. Gleicher, and S. Schunert. Recommendations for TREAT Historical Data to Validate MAMMOTH. Technical Report INL/MIS-16-37647, Idaho National Laboratory, January 2016.

[9] T. H. Bauer W. R. Robinson. The M8 Power Calibration Experiment (M8CAL). Technical Report ANL-IFR-232, Argonne National Laboratory, May 1994.

[10] W.R. Robinson and R.J. Page. TREAT NPR Calibration Experiment AN-CAL. Technical Report ANL-NPR-92-11, Argonne National Laboratory, September 1992.

[11] J. Leppänen. *Development of a New Monte Carlo Reactor Physics Code*. PhD thesis, Helsinki University of Technology, 2007.

[12] J. Ortensi et al. Deterministic modeling of the high temperature test reactor with DRAGON-HEXPEDITE. In *5th International Topical Meeting on High temperature Reactor Technology (HTR)*, Prague, Czech Republic, October 18 - 20 2010.

[13] J. Ortensi et al. Supercell depletion studies for prismatic high temperature reactors. In *6th International Topical Meeting on High temperature Reactor Technology (HTR)*, Tokyo, Japan, October 28 - Novermber 1 2012.

[14] Y. Wang. Nonlinear Diffusion Acceleration for the Multigroup Transport Equation Discretized with S_N and Continuous FEM with Rattlesnake. In *Proceedings to the International Conference on Mathematics, Computational Methods & Reactor Physics (M&C 2013)*, Sun Valley, Idaho, USA, May 2013.

[15] D. Andrs et al. RELAP-7 Level 2 Milestone Report: Demonstration of a Steady State Single Phase PWR Simulation with RELAP-7. Technical Report INL/EXT-12-25924, Idaho National Laboratory, 2012.

[16] R.L. Williamson et al. Multidimensional Multi-physics Simulation of Nuclear Fuel Behavior. *Jou. Nucl. Mat.*, 423(149–163), 2012.

[17] D.A. Knoll and D. E. Keyes. Jacobian-free Newton-Krylov Methods: a Survey of Approaches and Applications. *J. Comput. Phys.*, 193(2):357–397, 2004.

[18] V.A. Mousseau, D.A. Knoll, and W.J. Rider. Physics-Based Preconditioning and the Newton-Krylov Method for Non-equilibrium Radiation Diffusion. *J. Comput. Phys.*, 160:743–765, 2000.

[19] Y. Wang, H. Zhang, and R.C. Martineau. Diffusion acceleration schemes for self-adjoint angular flux formulation with a void treatment. *Nuclear Science and Engineering*, 176(2):201–205, February 2014.

[20] Randy Morris. Cubit 15.0 user documentation. Technical report, ETI, UT, 2014.

[21] J.E. Morel. A non-local tensor diffusion theory. Technical Report LA-UR-07-5257, Los Alamos National Laboratory, 2007.

[22] Proc. Int. Conf. on Mathematics and Computational Methods Applied in Nuclear Science and Engineering (MC 2011). *3-D Anisotropic Neutron Diffusion in Optically Thick Media with Optically Thin Channels*, Rio de Janeiro, Brasil, 2011.

[23] A. Kavenoky. The SPH Homogenization Method. In *IAEA Meeting on Homogenization Methods in Reactor Physics*, Lugano, Switzerland, 1978.

[24] A. Hébert. Développement de la methode SPH: Homogénéisation de cellules dans un réseau non uniforme et calcul des paramètres de réflecteur. Technical Report CEA-N-2209, Commissariat à l'Energie Atomique, 1981.

[25] A. Hébert. A Reformulation of the Transport-Transport SPH Equivalence Technique. In *7th International Conference on Modelling and Simulation in Nuclear Science and Engineering (7ICMSNSE)*, number 7, 2015.

[26] Tatsuya Fujita, Tomohiro Endo, and Akio Yamamoto. Application of correction technique using leakage index combined with SPH or discontinuity factors for energy collapsing on pin-by-pin BWR core analysis. *Journal of Nuclear Science and Technology*, 52(3):355–370, 2015.

[27] Mancang Li, Kan Wang, and Dong Yao. The Super Equivalence Method in Monte Carlo Based Homogenization. In *Proceedings of the 2014 22nd International Conference on Nuclear Engineering*, number 22. ICONE22, July 2014.

[28] Akio Yamamoto, Masahiro Tatsumi, Yasunori Kitamura, and Yoshihiro Yamane. Improvement of the SPH Method for Pin-by-Pin Core Calculations. *Journal of Nuclear Science and Technology*, 41(12):1155–1165, 2004.

[29] Go Chiba, Masashi Tsuji, Ken-ichiro Sugiyama, and Tadashi Narabayashi. A note on application of superhomogénéisation factors to integro-differential neutron transport equations. *Journal of Nuclear Science and Technology*, 49(2):272–280, 2012.

[30] Jimin Ma, Guanbo Wang, Shu Yuan, Hongwen Huang, and Dazhi Qian. An improved assembly homogenization approach for plate-type research reactor. *Annals of Nuclear Energy*, 85:1003 – 1013, 2015.

[31] E. Nikitin, E. Fridman, and K. Mikityuk. On the use of the SPH method in nodal diffusion analyses of SFR cores method in nodal diffusion analyses of sfr cores. *Annals of Nuclear Energy*, 85:544 – 551, 2015.

[32] P.N. Brown and Y. Saad. Hybrid Krylov Methods for Nonlinear Systems of Equations. *SIAM J. Sci. Stat. Comput.*, 11(3):450, 1990.

[33] J. Ragusa, R. Sanchez, and S. Santandrea. Application of Duality Principles to Reflector Homogenization. *Nuc. Sci. Eng.*, 157:299–315, 2007.

[34] Andreas Pautz. Improved Strategies for Fuel Assembly, Pin Cell and Reflector Cross Section Generation Using the Discrete Ordinates Code DORT. In *International Conference on Reactor Physics (PHYSOR)*, Cancouver, Canada, September 2006.


INL
Idaho National Laboratory